Bull. Disas. Prev. Res. Inst., Kyoto Univ., Vol. 32, Part 3, No. 291, 1982

Breaking Mechanism of Water Waves in Terms of Imbalance in the Partition of Wave Energies

By Yoshito TSUCHIYA and Shigeaki TSUTSUI

(Manuscript received May 6, 1982)

Abstract

A breaking mechanism of progressive waves on a sloping beach is investigated based on the change in partition rates of wave energies. When a wave propagates and approaches the breaking point, the potential energy initiates to decrease abruptly at a certain point where the radiation stress takes a maximum value, at the same time, the kinetic energy increases and becomes predominant in the wave. Therefore, the partition rate of wave energies becomes imbalanced and the wave falls into an unstable state as a whole. This premonitory phenomenon may lead to the breaking of waves.

1. Introduction

Accurate information of behaviour of water waves, especially the breaking of waves on a beach as the last stage of wave history, are essential for many applications in coastal engineering such as designs of nearshore structures and sand movements on a beach. Therefore many efforts have been made in order to clarify the breaking mechanism. It is thought however that both of the theoretical and experimental studies on the breaking phenomenon have fallen into trouble. We can not help accepting that accurate measurements, for instance measurements of water particle velocities in breaking waves, are still difficult because of the instantaneous behaviour of breaking waves.

Upon these circumstances, various breaking conditions have been employed. As the results of theoretical and experimental verifications of these conditions, a few facts concerning the breaking mechanism have been elucidated. These breaking conditions are 1) a relationship between the wave velocity and water particle velocity at the wave crest[1], 2) a relationship between the acceleration of gravity and that of a water particle at the wave crest[2], 3) occurrence of the cusp at the wave crest[1], 4) asymmetrical behaviour of wave profiles[3], and 5) experimental formulae such as the breaker index[4]. The last one is usually obtained by experiments to find breaker conditions. It may therefore be impossible to describe the whole history of breaking waves. The others deals with local conditions relating to the breaking phenomena.

Now, observing waves on a beach, one sees waves push up sand while advancing themselves, and throw the sand ahead simultaneously with breaking. Finally waves turn into flow. Considering this wave history, there may exist breaking conditions

which are subjected to not only the local conditions but the inner breaking conditions which integrate characteristics of waves. This is what the present paper aims to show.

There are some physical quantities such as the potential and kinetic energies, mass and energy fluxes, and radiation stress which are properties of the wave trains and have been completely defined. Several relationships between these integral properties have been developed[5]. Therefore, if some of these integral properties may be evaluated, we can discuss the inner characteristics of the wave train. In the present paper, we try to offer an inner breaking condition based on the instability of waves.

In Chapter 2, we formulate the problem and clearly explain our standpoints. Partition laws of wave energies are derived based on the conservation law of energy flux. In Chapter 3, the radiation stress and wave set-down are investigated. The radiation stress, defined as the excess momentum flux of waves, gradually increases with decrease in water depth, and takes place depression in the mean water level in front of the breaking points, that is, wave set-down. These phenomena may be deeply concerned with the breaking of waves. Nevertheless, only a formula for wave set-down[6], derived from the Stokes wave theory, has been proposed. Therefore it is necessary to develop the formula of wave set-down, which is applicable in the shallower regions. A formula is derived based on the balance of the momentum flux of waves by shallow water wave theories.

In Chapter 4, an experiment on breaking waves is described. The breaking waves are generated under the condition that the mass flux accompanied by the progressive waves is not restrained by the endwalls of a wave tank. Wave profiles in space are measured by a photographical method. Characteristics of shoaling waves such as changes in wave height and length are made clear by comparison with theoretical estimations, and some of the previous breaking conditions are also described. The ever-changing potential energy, which is the only single integral property directly measurable by experiments, can be estimated. Changes in potential and kinetic energies of shoaling waves are discussed to investigate the phenomena which may occur in just breaking waves based on the imbalance of the partition rate of these two energies. By the comparison of experimental and theoretical results, the essential points of difference between them are considered to show that there possibly exists an inner breaking condition, as mentioned already.

2. Partition Rates of Wave Energies in Breaking of Progressive Waves

Consider two-dimensional, surface waves propagating under the influence of gravity, g, on a fluid of constant density, ρ. Assume that the fluid is inviscid and incompressible and that the motion is irrotational. The waves are also assumed to be propagated on water of gradually varying depth, h. Let the potential energy, kinetic energy, and group velocity be denoted by E_p, E_k, and c_g, respectively.

In case the energy flux of the waves is conserved (energy flux method), the con-

servation law $(E_p+E_k)c_g=$const. leads to

$$\frac{E_k}{E_{ki}}=\frac{c_{gi}}{c_g}+\frac{E_{pi}}{E_{ki}}\left(\frac{c_{gi}}{c_g}-\frac{E_p}{E_{pi}}\right) \quad \cdots\cdots(1)$$

where the subscript i denotes quantities of offshore waves (incident waves). The partition rate of wave energies, that is, the ratio of the kinetic to potential energy becomes

$$\frac{E_k}{E_p}=\frac{c_{gi}}{c_g}\frac{E_{pi}}{E_p}\left(\frac{E_{ki}}{E_{pi}}+1\right)-1 \quad \cdots\cdots(2)$$

Now consider the waves in the region where the condition,

$$kh\gg 1 \quad \cdots\cdots(3)$$

is satisfied, in which k is the wave number. In the region it is usually considered sufficient to evaluate the partition rate in the incident waves to equal unity, that is,

$$\frac{E_{ki}}{E_{pi}}=1 \quad \cdots\cdots(4)$$

Therefore Eqs. (1) and (2) can be transformed respectively into

$$\frac{E_k}{E_{ki}}=2\frac{c_{gi}}{c_g}-\frac{E_p}{E_{pi}} \quad \cdots\cdots(5)$$

$$\frac{E_k}{E_p}=2\frac{c_{gi}}{c_g}\frac{E_{pi}}{E_p}-1 \quad \cdots\cdots(6)$$

These equations govern the partition laws of wave energies until the waves break.

Since the wave energy flux method has often been employed in the calculation of wave shoaling, let us show an example of the calculated results of Eqs. (5) and (6). Changes in physical quantities such as the potential and kinetic energies, wave length, wave height, and group velocity are shown in **Fig. 1.** Theories adopted are the Stokes wave theory of third order approximation (S-3)[7] based on the Stokes first definition of the wave velocity, Quasi-Stokes wave theory (QS-4)[8] and cnoidal wave theory (NC-3)[9], the last two of which have been derived by the reductive perturbation method. The co-ordinate origin is taken at a point on the shoreline with the x-axis horizontally offshoreward as shown **Fig. 1,** and H, L, T, h_b, and θ are the wave height, wave length, wave period, breaking depth, and gradient of a beach slope, respectively. The subscript o denotes the quantities for deep water waves. Further, in the figure, the breaking conditions employed are the so-called Rankine-Stokes' breaking condition and the breaker index[4].

From this figure, it is found that the wave length and group velocity decrease in shallower regions, $x/h_b<10^3$, as the wave propagates over the sloping beach, but on the contrary, the others increase monotonically until the wave breaks. This example of $E_k/E_p\fallingdotseq 1.14$ at the breaking point leads to the fact that the kinetic energy is slightly larger than the potential one.

In order to verify these theoretical inner characteristics, the physical quantities in Eqs. (5) and (6) should be investigated experimentally. However, the change in

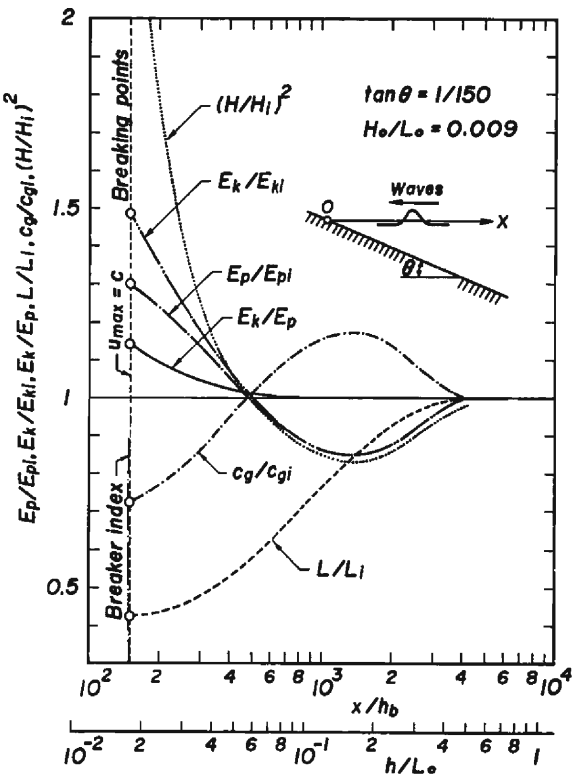

Fig. 1 Changes in physical quantities of a shoaling wave.

potential enrgy, E_p/E_{pi}, is only determined directly in these quantities. If the wave profiles of shoaling waves are experimentally measured in space the potential energy can be estimated by the definition

$$E_p=\frac{\rho g}{L}\int_0^L \frac{1}{2}\eta^2\, dx \qquad \cdots\cdots(7)$$

where η is the water surface displacement from the mean water level. As the wave energy flux is conserved, if the change in group velocity, c_g/c_{gi}, is evaluated from a proper way, it is possible to determine the partition rate of wave energies, E_k/E_p, near the breaking point based on Eq. (6). Consequently we can discuss the partition of wave energies of shoaling waves to find an inner breaking condition.

3. Wave Set-Down

One of the most important wave-driven effects occurs when waves encounter a sloping beach. The waves shorten, steepen, and eventually break. In the steady state, the shoreward flux of momentum must be independent of x, which is taken perpendicular to the shore. It is well known that the resulting change in the radiation stress produces change in the level of mean water, that is, wave set-down.

Let the horizontal and vertical components of water particle velocities, the pressure and the time be u, w, p, and t, respectively. The radiation stress[11] is defined by

$$S=\frac{1}{T}\int_0^T\int_0^{h+\eta}(p+\rho u^2)\,dzdt-\frac{1}{2}\rho gh^2-\frac{1}{\rho h}\left(\frac{1}{T}\int_0^T\int_0^{h+\eta}\rho u\,dzdt\right)^2 \quad \cdots\cdots(8)$$

where z is the vertical co-ordinate measured upward from the sea bottom. For Stoke waves Eq. (8) leads to

$$\begin{aligned}\frac{S}{\rho gh^2}=&\frac{1}{2}\left(\frac{a}{h}\right)^2\left(1+\lambda^2\frac{8ch^4-8ch^2+9}{8sh^4}\right)\left(\frac{kh}{shch}+\frac{1}{2}\right.\\&+\lambda^2\left\{\frac{-20ch^8+36ch^6-12ch^4+5ch^2-9}{16sh^8}\,\frac{kh}{shch}\right.\\&\left.\left.+\frac{20ch^6-28ch^4+35ch^2-18}{32sh^6}\,\frac{shch}{kh}\,\frac{1}{2sh^2}\right\}\right)\end{aligned} \quad \cdots\cdots(9)$$

where a and λ are parameters concerned with wave properties, and the notation for brevity is made so that $sh=\sinh kh$ and $ch=\cosh kh$.

Longuet-Higgins and Stewart[6] have integrated the equation of horizontal momentun balance to yield the formula of wave set-down, Δh, as

$$\frac{\Delta h}{d}=-\frac{1}{4}\left(\frac{a}{d}\right)^2\frac{2kd}{\sinh 2kd} \quad \cdots\cdots(10)$$

where d is the local depth of water. In Eq. (10) the lowest order term of the radiation stress of Eq. (9) is adopted, and the local depth, d, is assumed to be nearly equal to the mean depth, h. This formula has the validity of approximation only in the region where the Stokes wave theory is applied. Therefore simular formulae of wave set-down must be developed in shallower regions where proper wave theories, for example the cnoidal wave theory, are applicable.

Based on Eq. (8), the radiation stresses for Quasi-Stokes waves of the fourth order approximation and cnoidal waves of the third order are expressed[10] respectively as

$$\frac{S}{\rho gh^2}=\frac{\lambda_0^2}{16}\left(3-\frac{2}{3}(kh)^2+\frac{14}{45}(kh)^4-\frac{57}{1890}(kh)^6+\frac{3}{64}\lambda_0^2\{3(kh)^{-4}+10(kh)^{-2}\}\right) \quad \cdots\cdots(11)$$

$$\begin{aligned}\frac{S}{\rho gh^2}=&\frac{\lambda^2}{2k^4}\left(-\left(\frac{E}{K}\right)\left\{3\left(\frac{E}{K}\right)+2k^2-4\right\}+k^2-1\right)\\&+\frac{\lambda^3}{10k^6}\left(100\left(\frac{E}{K}\right)^2\left\{\left(\frac{E}{K}\right)+k^2-2\right\}+2\left(\frac{E}{K}\right)(11k^4-61k^2+61)\right.\\&\left.-11(k^4-3k^2+2)\right)+\frac{\lambda^4}{4200k^8}\left(-25\left(\frac{E}{K}\right)^3\left\{3339\left(\frac{E}{K}\right)+4488k^2-8904\right\}\right.\\&-50\left(\frac{E}{K}\right)^2(861k^4-4200k^2+4200)-100\left(\frac{E}{K}\right)(49k^6-504k^4\\&\left.+1218k^2-812)+(2450k^6-12775k^4+20650k^2-10325)\right)\end{aligned} \quad \cdots\cdots(12)$$

where k^2 is the modulus of Jacobian elliptic functions, K and E are the complete elliptic integrals of the first and second kinds, respectively, and λ_0 and λ the parameters

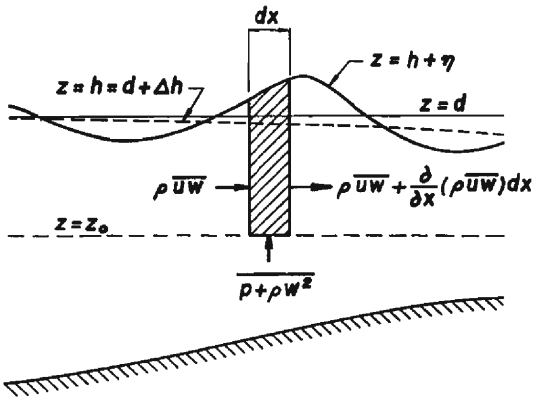

Fig. 2 Vertical momentum balance in a shoaling wave.

which are the function of wave properties.

Since these two expressions for the radiation stress are too complicated to reduce formulae of wave set-down in the similar way as Longuet-Higgins and Stewart, let us investigate the general relation for the vertical momentum flux and propose a formula for wave set-down.

Consider the vertical momentum balance in a section of water bounded by the surface, $z=h+\eta$, a horizontal plane, $z=z_0$, and two vertical planes, $x=x_0$ and $x=x_0+dx$, as shown in **Fig. 2.** The mean flux of vertical momentum (per unit corss-section) across the horizontal plane is given by

$$\overline{p+\rho w^2}-\frac{\partial}{\partial x}\overline{\int_{z_0}^{h+\eta}\rho uw\ dz}$$

in terms of the pressure and Reynolds stresses, in which the over-bar denotes the time average. This average flux of momentum must balance the total weight of the section of water, so that the relation for the vertical momentum flux can be obtained.

$$\left.\begin{aligned}\overline{p+\rho w^2}-\frac{\partial}{\partial x}\overline{\int_{z_0}^{h+\eta}\rho uw\ dz}&=\bar{p}_0+\overline{\rho g(h+\eta-z_0)}\\ p_0&=\rho g(h-z_0)\end{aligned}\right\}\quad\cdots\cdots(13)$$

On the other hand, taking time average in the Bernoulli equation, we have

$$\rho\overline{\frac{\partial\phi}{\partial t}}+\bar{p}+\frac{1}{2}\rho\overline{(u^2+w^2)}+\rho g\overline{(z_0-h)}=\overline{f(t)}=\text{const.}\quad\cdots\cdots(14)$$

where ϕ is the velocity potential, $f(t)$ a certain function of time. From Eqs. (13) and (14) we may have

$$\rho g(h-d)=-\frac{1}{2}\rho\overline{(u^2-w^2)}-\rho\overline{\frac{\partial\phi}{\partial t}}-\frac{\partial}{\partial x}\overline{\int_{d}^{h+\eta}\rho uw\ dz}+C\quad\cdots\cdots(15)$$

at the still water level, $z_0=d$, where C is a constant. This equation expresses the time average of vertical momentum flux at the still water level, thus likely giving the wave set-down for any point of x.

The terms contained in Eq. (15) can be evaluated as follows: The velocity potential for Stokes waves is determined such that the relation $C=\overline{\rho\partial\phi/\partial t}$ must be held[6,11]. In the Quasi-Stokes and cnoidal wave theories[10], the horizontal water particle velocity is given by

$$\left.\begin{aligned} u&=\frac{\partial\phi}{\partial x}=\bar{u}+\sum(\text{periodic terms})\\ \bar{u}&=\frac{1}{T}\int_0^T u\,dt\neq 0\end{aligned}\right\} \quad\cdots\cdots(16)$$

Thus the velocity potential becomes

$$\phi=\bar{u}x+\int\sum(\text{periodic terms})\,dx \quad\cdots\cdots(17)$$

in which the secular term is determined to have vanished. Therefore the time-averaged term, $\overline{\partial\phi/\partial t}$, vanishes in these two theories. The constant, C, is also null in the basic equations.

In evaluating the third term of Eq. (15), the slope is assumed to be sufficiently gentle such that the reflection of waves is of neglegible importance in the case of calculation of shoaling waves. Therefore the order of approximation of the derivative with respect to x may lead to

$$\frac{\partial}{\partial x}\overline{\int_d^{h+\eta}\rho uw\;dz}\cong\frac{\partial}{\partial x}\overline{\int_h^{h+\eta}\rho uw\;dz} \quad\cdots\cdots(18)$$

It is higher than the highest order of the theories employed, and so this term is also neglegible. Consequently the wave set-down, $\Delta h=h\text{-}d$, may be evaluated by

$$g\Delta h\cong-\frac{1}{2}\overline{(u^2-w^2)} \quad\cdots\cdots(19)$$

under the condition that $z=d\cong h$.

Substituting the known relations of the water particle velocities for the Stokes, Quasi-Stokes, and cnoidal waves in Eq. (19), we obtain for the Stokes wave theory

$$\begin{aligned}\frac{\Delta h}{h}=&-\frac{1}{4}\left(\frac{a}{h}\right)^2\frac{kh}{shch}\left(1+\lambda^2\frac{8ch^4-8ch^2+9}{8sh^4}\right)\\&\times\left(1+\lambda^2\frac{-20ch^6+16ch^4+4ch^2+9}{16sh^6}\right)\end{aligned} \quad\cdots\cdots(20)$$

for the Quasi-Stokes wave theory

$$\begin{aligned}\frac{\Delta h}{h}=&-\frac{\lambda_0^2}{16}\left(1-\frac{2}{3}(kh)^2+\frac{14}{45}(kh)^4-\frac{461}{3870}(kh)^6\right.\\&\left.+\frac{3}{64}\lambda_0^2\{3(kh)^{-4}-7(kh)^{-2}\}\right)\end{aligned} \quad\cdots\cdots(21)$$

and for the cnoidal one

$$\begin{aligned}\frac{\Delta h}{h}=&-\frac{\lambda^2}{6k^4}\left(-\left(\frac{E}{K}\right)\left\{3\left(\frac{E}{K}\right)+2k^2-4\right\}+k^2-1\right)\\&-\frac{\lambda^3}{30k^6}\left(75\left(\frac{E}{K}\right)^2\left\{\left(\frac{E}{K}\right)+k^2-2\right\}+\left(\frac{E}{K}\right)(14k^4-89k^2+89)\right.\end{aligned}$$

$$-7(k^2-1)(k^2-2)\Big)-\frac{\lambda^4}{2100k^8}\Big(-175\Big(\frac{E}{K}\Big)^3\Big\{129\Big(\frac{E}{K}\Big)+188k^2-352\Big\}$$

$$-2\Big(\frac{E}{K}\Big)^2(6307k^4-30982k^2+29582)+4\Big(\frac{E}{K}\Big)(247k^6-3524k^4$$

$$+8740k^2-5710)+(k^2-1)(494k^4-2701k^2+2701)\Big) \quad \cdots\cdots(22)$$

respectively.

Eq. (10) coincides with Eq. (20) in the lowest order of approximation, assuming that the local depth nearly equals the mean water depth, h. By comparison of Eqs. (11) and (12) with Eqs. (21) and (22), respectively, it is noted that the wave set-down is about one-third of the radiation stress in the shallower region. The resulting changes in the radiation stress and wave set-down, expressed by Eqs. (9) to (12) and Eqs. (20) to (22) will be discussed in the next chapter comparing them with experimental results.

4. Experiments on Breaking Waves

4.1 Experimental apparatus and procedures

(1) Wave tank

If physical quantities in beaking waves abruptly change, it may be impossible to measure the breaking properties such as water particle velocities near the water surface and wave profiles. It is also well known that the breaker-type of waves which may be discussed based on the shallow water theory is a so-called spilling breaker occurring on water of gradually varying depth. Therefore, it is convenient for the experiment that the gradient of the slope is as mild as possible. In this study it was determined as 1/150.

The wave tank used in this experiment is a double-deck type as shown in **Fig. 3,**

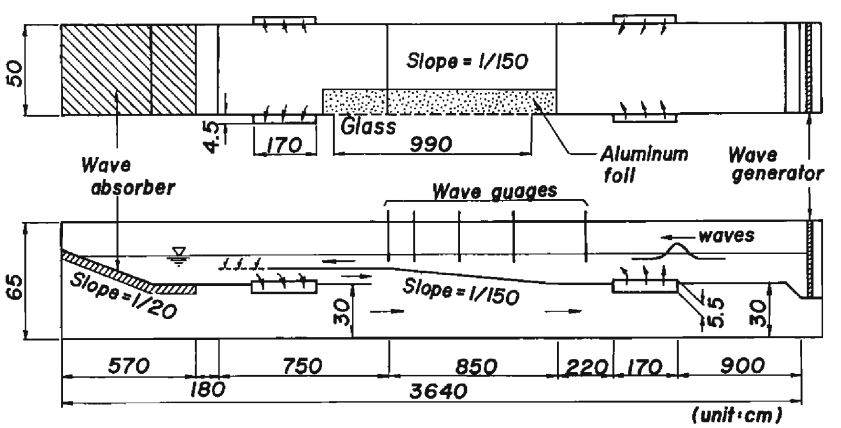

Fig. 3 Wave tank of double-deck type.

belonging to the Ujigawa Hydraulics Laboratory, Disaster Prevention Research Institute, Kyoto University. The slope is located in the middle position of the wave tank. Water depths of the front and rear sides of the slope are constants, and the latter is determined under the condition that the waves should break at the end of the slope. The mass flux accompanied by the wave is returned to the wave generater-side through a circulating duct between the upper and lower decks. By using these apparatuses, the mass transport of waves is not constrained by the endwall of the wave tank; furthermore, the breaking properties such as the breaking point, wave heights, and wave profiles become steady. This wave tank then can properly carry out the purpose of the present study.

There exists the observational glass window on one side of the wave tank with a mesh 2 cm vertically by 4 cm horizontally. This mesh is used as the basic line for measurements of the surface displacements by photographs.

(2) Measurements of breaking properties

In this experiment, wave profiles in time and in space over the slope are measured after the properties of breaking waves are made steady.

a. Steadiness of the properties of waves

Wave gauges are set up at six locations in the wave tank as shown in **Fig. 4**, and the wave records are continuously obtained from the beginning of wave generation. The steadiness is confirmed based on the wave records under the condition that wave heights become uniform at measured points and that harmonic changes in wave heights do not appear at the breaking point. However the changes in wave height within 2 mm at the breaking point may be considered to be allowable. The starting time of measurements is one hour after wave generation in all runs.

b. Wave profiles in time and in space

Wave profiles in time are measured by wave gauges, which are set up in the wave tank as shown in **Fig. 4.**

Wave profiles in space are measured by a photographical method as shown in **Fig. 5.** The motor-driven carriage is set up about 3 m apart from the glass window and parallel to the axis of the wave tank. This carriage can move with a constant speed being nearly equal to the measured mean wave velocity. Photographs of wave profiles over the slope are taken by means of 35 mm camera (3 frames per second) through the glass. This procedure is carried out three times in each run. The negative films are magnified as large as the prototype and projected on a screen. Water surface displacements are measured at an interval of 1 cm near the wave crest

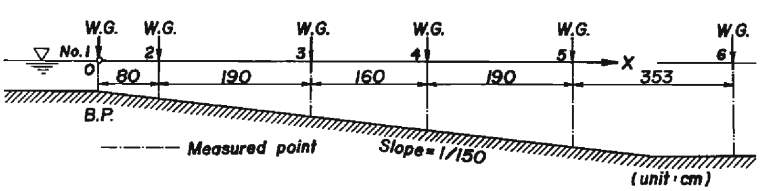

Fig. 4 Measured points.

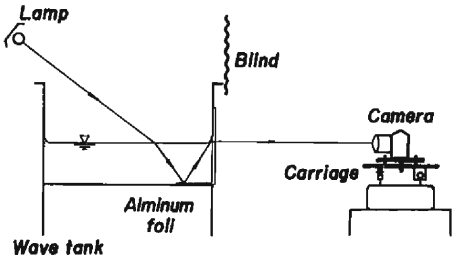

Fig. 5 Photographical method for wave profiles in space.

and 2 cm near the wave trough, respectively.

Also there is a simple device to take sharp pictures of wave profiles, as shown in **Fig. 5.** Thin alminum foil 10 cm in width is pasted up on the bottom of the wave tank in order to reflect the light from the opposite side. This reflected light is again scattered by the meniscus on the glass, and the illuminant meniscus is caught by means of the camera on the carriage.

c. Wave lengths

Wave lengths for the calculation of the potential energy are defined as the distance between two adjacent wave crests from wave profiles in space.

d. Wave set-down

Depressions of the mean water level, that is, wave set-downs are defined as the difference between the still and mean water levels measured from wave profiles in space.

The experimental conditions at the breaking point, and physical parameters of the first wave over the slope are given in **Tables 1** and 2, respectively.

Table 1 Experimental conditions at the breaking point.

Run	$T\sqrt{g/h_b}$	H_b/h_b
1	13.8	0.734
3	11.2	0.684

Table 2 Physical parameters of incident waves over the slope.

Run	$T\sqrt{g/h}$	H/h	h/L_0	H_0/L_0	Adopted theories
1-1	10.3	0.313	0.0589	0.0182	
1-2	10.3	0.300	0.0596	0.0181	QS-4
1-3	10.3	0.323	0.0594	0.0189	
3-1	8.15	0.295	0.0938	0.0293	
3-2	8.08	0.312	0.0954	0.0315	S-3
3-3	8.26	0.293	0.0914	0.0283	

4.2 Experimental results and discussion

In this section, the properties of breaking waves such as the changes in wave height, wave length, and steepness due to wave shoaling are clarified, and the breaking mechanism is discussed based on the imbalance of the partition rate of wave energies, and on the comparison with the changes in radiation stress and wave set-down.

(1) Characteristics of breading waves

a. Wave profiles in time and in space

Photo. 1 shows an example of wave profiles in space. **Fig. 6** shows examples of wave profiles in space which were measured for Runs 1 and 2 with these photographs, in which x' is the distance when the co-ordinate origin is taken in phase with the wave crest. Hereafter the co-ordinate origin is located at the end point of the slope for the convenience of comparisons of experimental and theoretical results. The curves are theoretical ones based on the Stokes, Quasi-Stokes, and cnoidal wave theories.

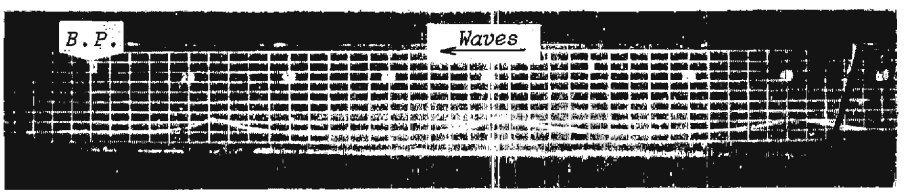

Photo. 1 Example of wave profiles in space (Run 3).

In Run 1, wave profiles near the wave crests are roughly symmetrical in the deeper region, and conserve this symmetry even if in the shallower region. The symmetry of wave profiles is slightly marred at the breaking point. In Run 3, the figure well shows that the wave profiles in the offshore region are symmetrical but become asymmetrical due to wave shoaling. In both of these Runs, the theoretical wave profiles are in accordance with experimental ones in the offshore region. However it is remarkable that the asymmetrical wave profiles near the breaking point can not be simulated by the theories even in case of the sufficiently mild slope of 1/150.

In the previous studies on breaking waves, wave profiles in time have frequently been employed as the experimental wave profiles. Nevertheless wave profiles in time and in space may be different. Therefore it is significant to compare these two wave profiles in order to clarify the breaking phenomenon. **Fig. 7** shows examples of wave profiles in time and in space for Runs 1 and 3, where the measured points, x/h_b, are nearly equal to each other. Two values of x/h_b and H/h are given in the figure respectively. Values in bracket are those corresponding to wave profiles in space. In these Runs, the asymmetry of wave profiles in space is more remarkable than those in time. It is however necessary to investigate in detail about these relationship between wave profiles in time and in space.

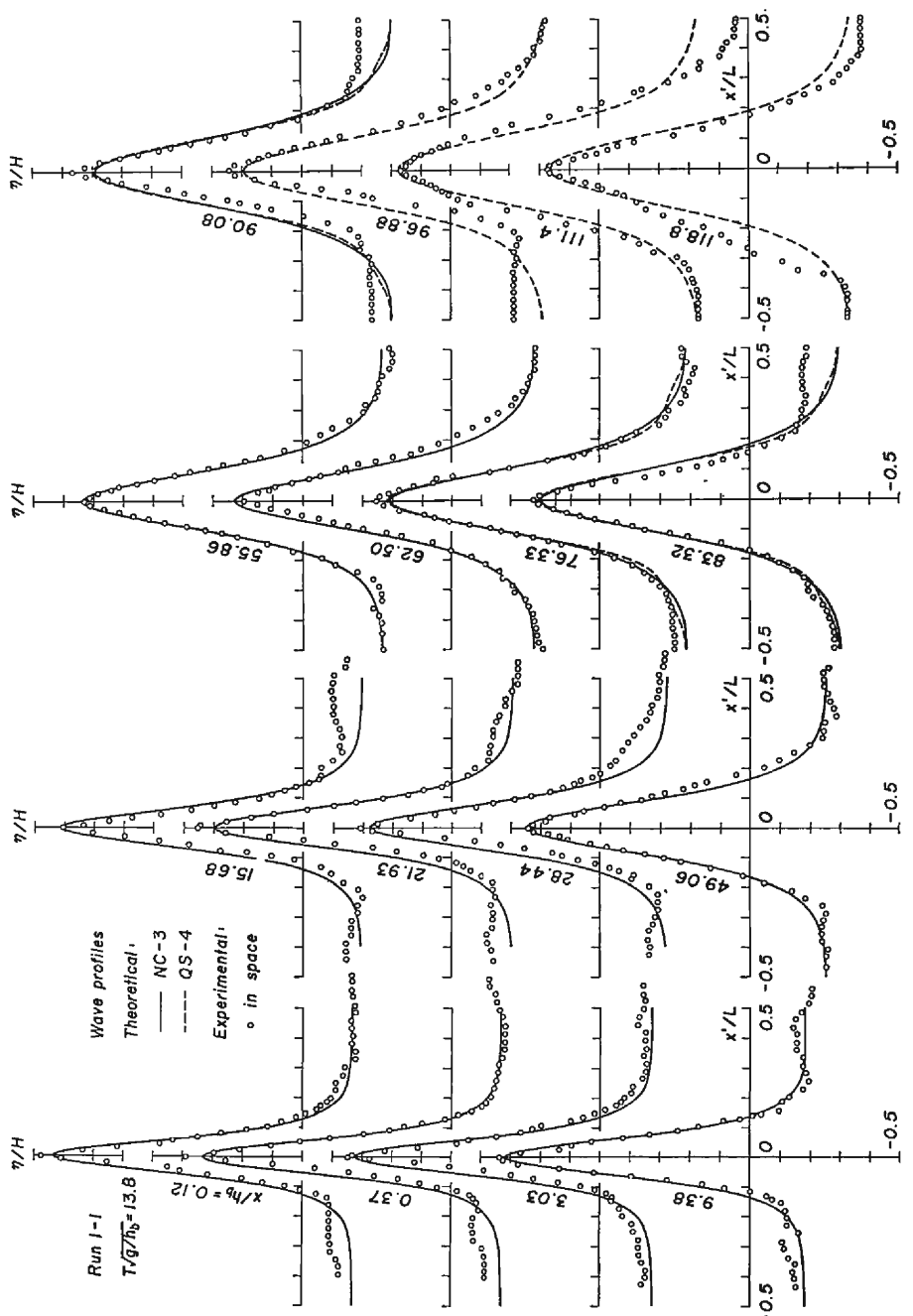

(1) Run 1

Fig. 6 Comparison of wave profiles in space with theoretical ones.

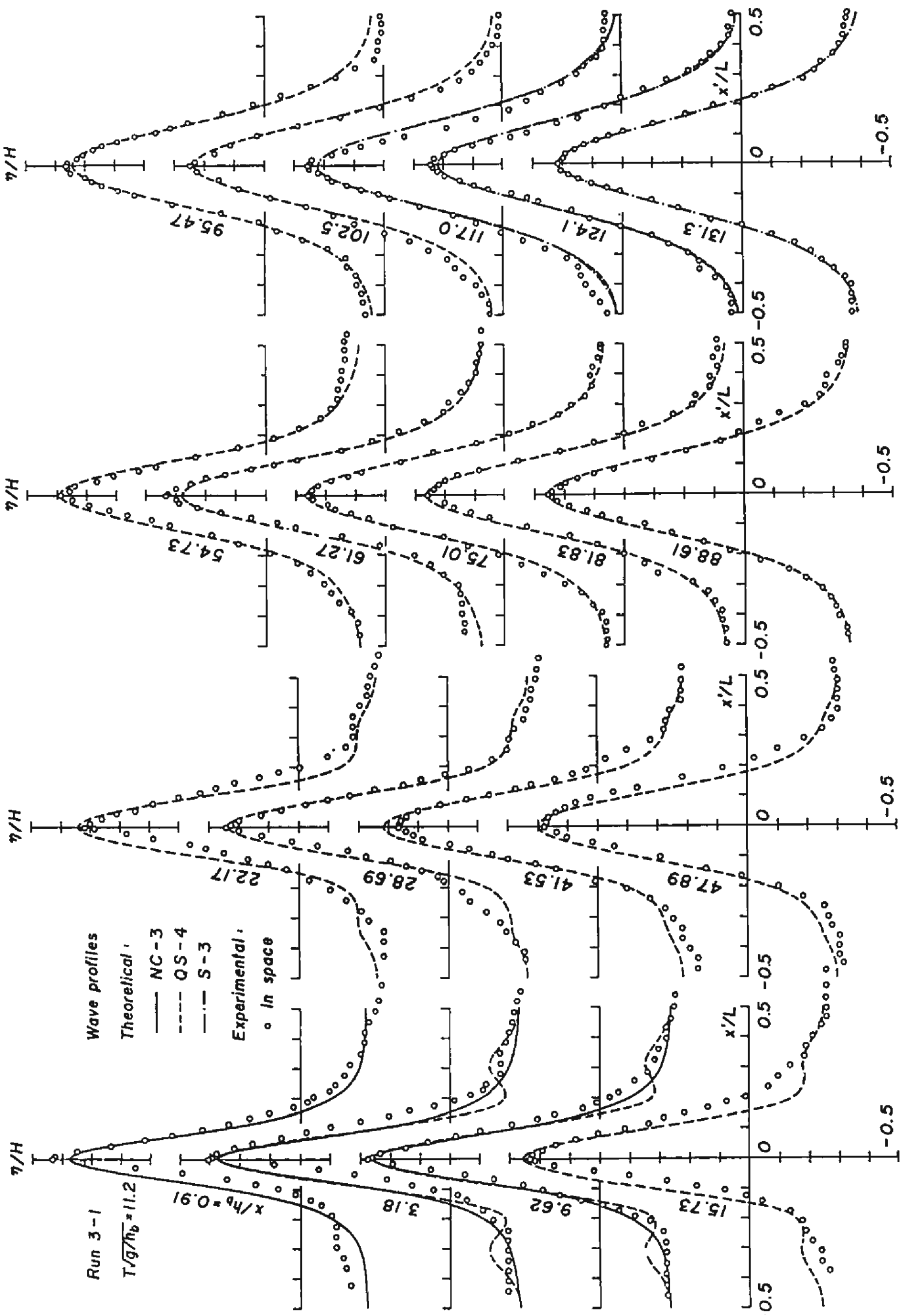

(2) Run 3

Fig. 6 Continued.

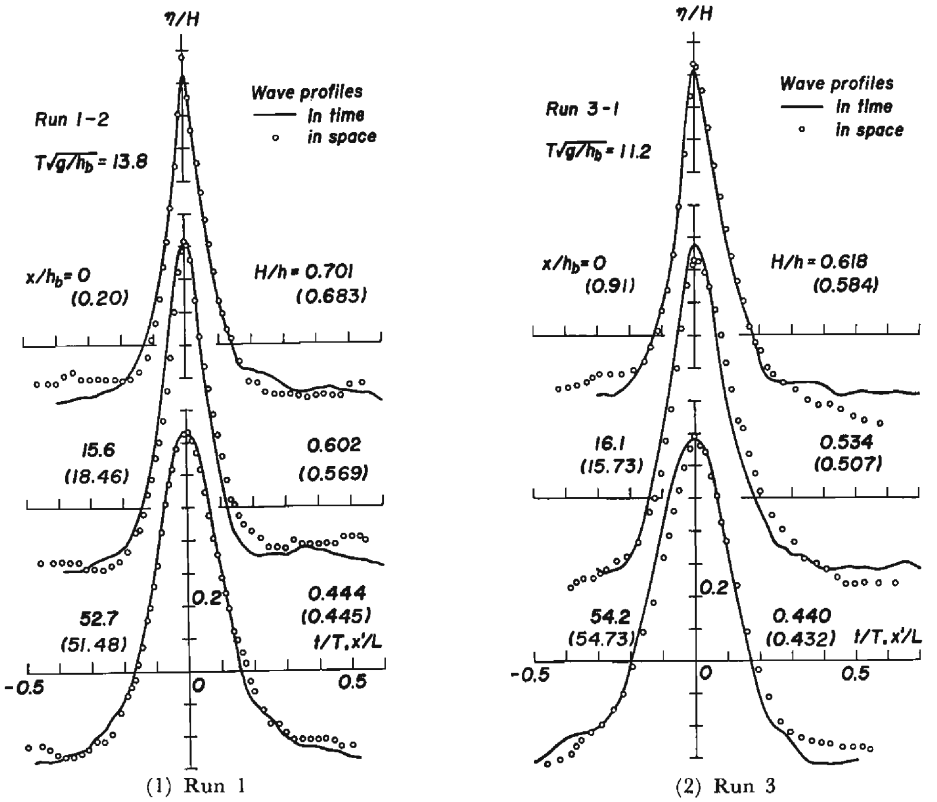

(1) Run 1 (2) Run 3

Fig. 7 Comparison of wave profiles in time and in space.

b. Changes in wave length

Changes in wave length over the slope are shown in **Fig. 8.** The thick lines in the figure are experimental curves, and the thin lines are theoretical ones based on the wave energy flux method. Also in these theoretical curves, the broken and solid lines correspond to wave lengths evaluated by the employment of wave heights

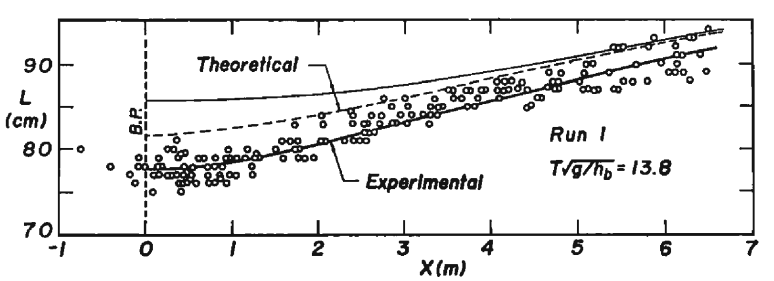

(1) Run 1

Fig. 8 Changes in shoaling wave length over the slope.

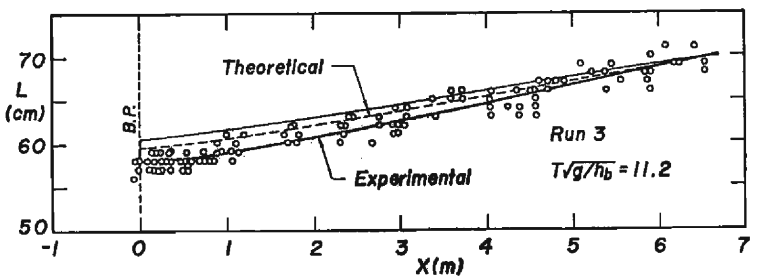

(2) Run 3

Fig. 8 Continued.

of the first wave in space over the slope, and those of the waves in time at the measured point 5, respectively. There are differences in the theoretical curves because of the discrepancy in the incident wave heights.

Experimental wave lengths agree well with theoretical ones in the deeper region and the former becomes slightly shorter than the latter due to the decrease in water

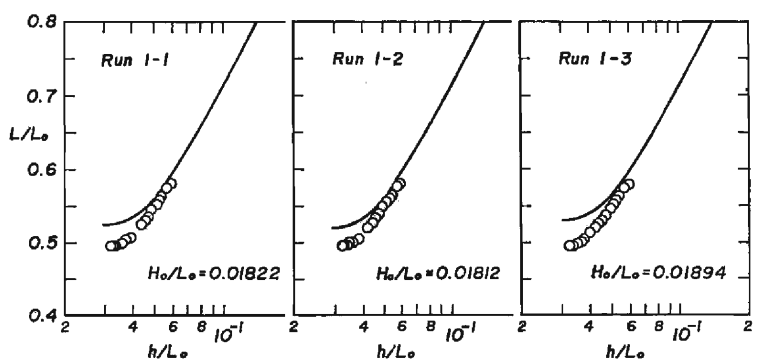

(1) Run 1

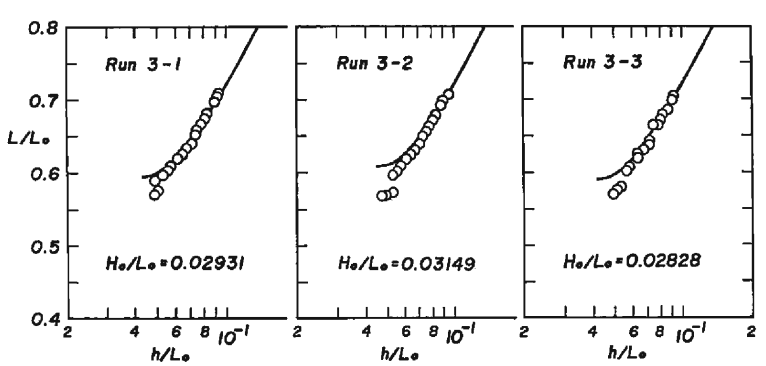

(2) Run 3

Fig. 9 Changes in shoaling wave length.

depth. Wave lengths in the calculation of the potential energy are determined from these experimental curves. The measurement errors in wave lengths are within about five percent.

Fig. 9 shows the changes in wave length for the particular waves given in **Table 2**, which will be discussed in the next section. In both of Runs 1 and 3, measured wave lengths are shorter than the theoretical ones near the breaking point, but the experimental tendency of the changes in wave length due to the decrease in water depth is very similar to the theoretical one.

c. Changes in wave height

Changes in wave height with varying depths is shown in **Fig. 10**, in which the symbol of a solid circle denotes wave heights obtained from wave profiles in time, the broken line shows the corresponding theoretical curves, and the steepness of deep water waves are shown in brackets.

Apart from some slight irregularity in wave height, experimental wave heights coincide with theoretical ones in the offshore region in both Runs 1 and 3. The former is slightly smaller than the latter near the breaking point. There is nearly

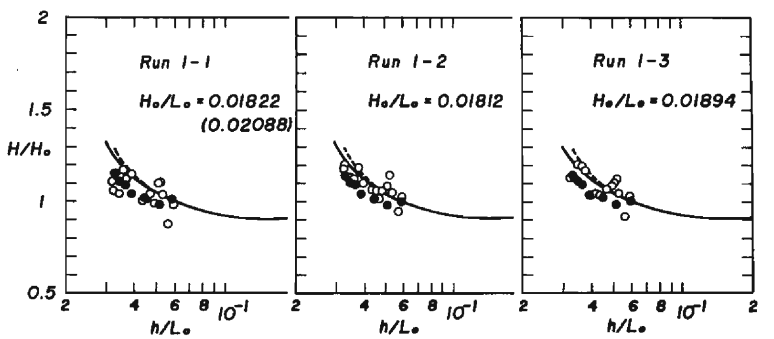

(1) Run 1

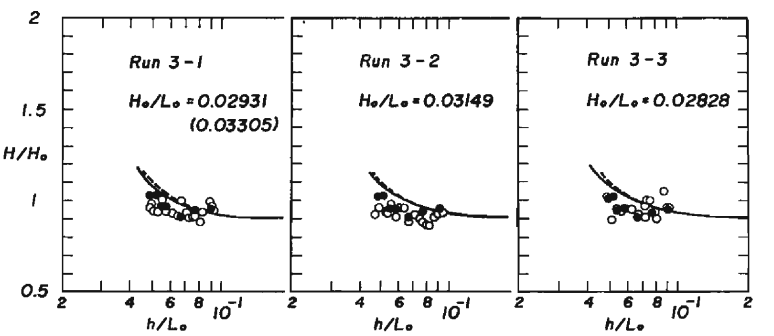

(2) Run 3

Fig. 10 Changes in shoaling wave height.

the same tendency as in the changes in wave length. The chief cause of these irregularities of wave height may be due to the photographical measurement error for wave profiles. Seen from observational points, as waves approach the breaking point, wave crests become steep, and the dynamic condition near the wave crest is similar to that of wave fronts propagating over a dry-bed. Therefore, these phenomena occasionally occurred near the breaking point at which pictures very close to the wave crest lack clearness.

d. Changes in steepness

The relationships between the wave height and wave length are shown in **Fig. 11.** As shown above in **Figs. 9** and **10,** experimental wave lengths and wave heights are both slightly smaller than the theoretical ones near the breaking point. Nevertheless, these experimental values of steepness agree very closely with the theoretical ones over almost the whole range of wave lengths. Theoretical breaking depths are shallower than the experimental ones as seen in **Fig. 9.** However, by the employment of the representation of h/H versus L/h, the influence of these discrepancies in breaking depth does not apparently arise, and this is the reason why the characteristics of the changes in steepness due to the varying depth well coincide.

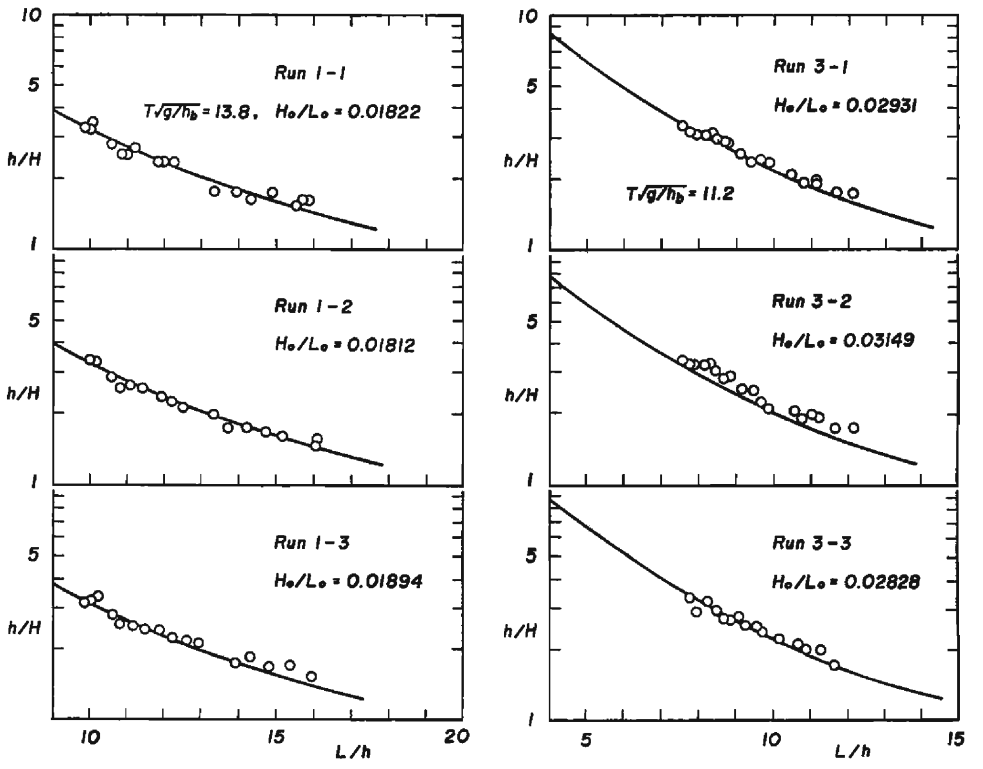

(1) Run 1 (2) Run 3

Fig. 11 Changes in shoaling wave steepness.

e. Breaking conditions

The results of the experimental investigations on the local breaking conditions, from the previous work presented by investigators[12], the following facts are summarized.

i) Rankine-Stokes' breaking condition

By the comparison of the maximum, horizontal component of water particle velocities on the water surface with the wave velocity, which is defined by the ratio between the wave length and wave period, it is found that both of these values become equal at the breaking point, that is, Rankine-Stokes' breaking condition is satisfied.

ii) Breaking wave heights

Experimental breaking wave heights have smaller values of about ten percent than theoretically evaluated values based on the wave energy flux method with Rankine-Stokes' breaking condition. Furthermore, experimental ones have smaller values than those of the breaker index by four percent. However, judging from the accuracy of the breaker index, both of these experimental and theoretical values may well agree.

iii) Breaking angles

The type of breaking waves is a so-called spilling breaker, and the angles of wave crest at just breaking are ninety to ninety-three degrees. According to Schwartz[13], waves with breaking angles of about ninety degrees predominate in deep water. Therefore these experimental angles may be reasonable even if in water of finite depth.

(2) Occurrence of the breaking of waves subjected to the imbalance in the partition of wave energies

To estimate the left sides of Eqs. (5) and (6), which govern the partition of wave energies, measurements of the changes in group velocity is required. Since it is impossible to measure the changes directly, at this stage we adopt an approximation as follows.

Fig. 12 shows the theoretical results of the changes in potential and kinetic energies, radiation stress, group velocity, wave length, and wave height. Experimental curves for wave lengths are also added in this figure. These experimental and theoretical results of wave length coincide over the whole range of the distance, x/h_{bt}, within an error of five percent. Assuming that the wave period does not change with the varying depth, the changes in wave length, L/L_i, equal those in wave velocity, c/c_i. Therefore the changes in group velocity, c_g/c_{gi}, may be approximated by the changes in wave length, L/L_i, near the breaking point, that is,

$$\frac{c_g}{c_{gi}} \cong \frac{L}{L_i} = \frac{c}{c_i} \quad \cdots\cdots (23)$$

On the other hand, according to the theoretical results, the partition rates of incident waves, E_{ki}/E_{pi}, for Runs 1 and 3 equal 1.027 and 1.029, respectively. This means that the assumption of Eq. (4) is approximately satisfied by the experimental incident waves.

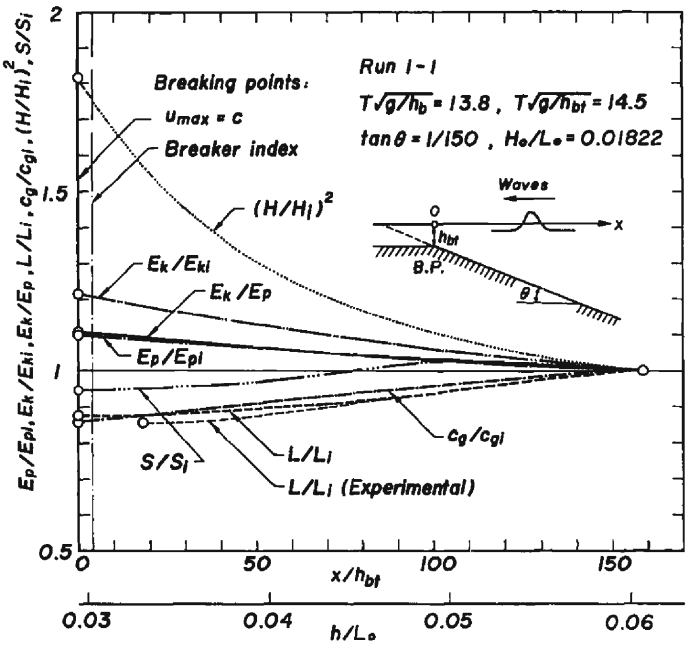

(1) Run 1

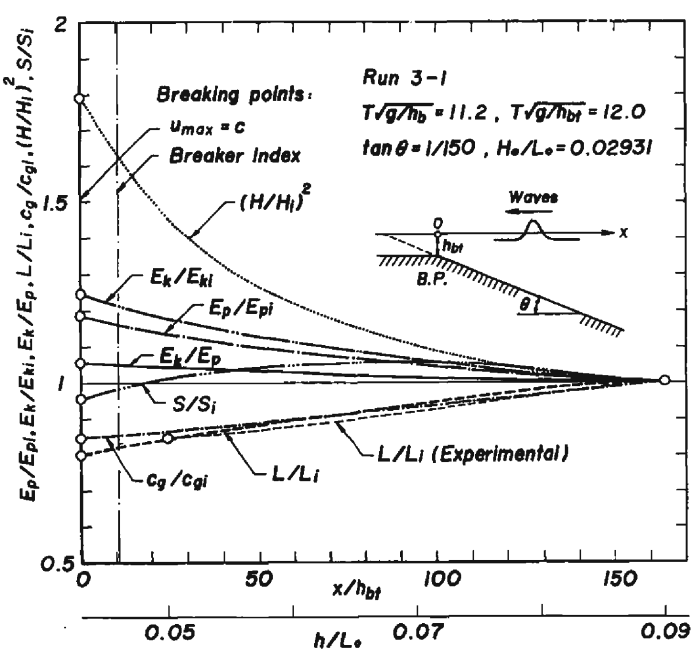

(2) Run 3

Fig. 12 Changes in physical quantities of the shoaling wave.

Therefore Eqs. (5) and (6) can be approximated by

$$\frac{E_k}{E_{ki}} \cong 2\frac{c_i}{c} - \frac{E_p}{E_{pi}} \quad \cdots\cdots (24)$$

and

$$\frac{E_k}{E_p} \cong 2\frac{c_i}{c}\frac{E_{pi}}{E_p} - 1 \quad \cdots\cdots (25)$$

respectively.

Fig. 12 shows that the wave length, L/L_i, and group velocity, c_g/c_{gi}, both decrease with wave shoaling, while the energies, E_p/E_{pi}, E_k/E_{ki}, and E_k/E_p, and wave height, $(H/H_i)^2$, all increase together until the waves break. Among them, it is well worth remarking that the radiation stress, S/S_i, takes a maximum value at certain points of h/L_0, and its change differs from the monotonical change in the other physical quantities. The nondimensional radiation stress, $S/\rho gh^2$, increases toward the breaking point as shown in **Fig. 13**. However the increasing rate are depressed after certain points of h/L_0 (marked by a symbol; ↓). This is the reason why the radiation stress

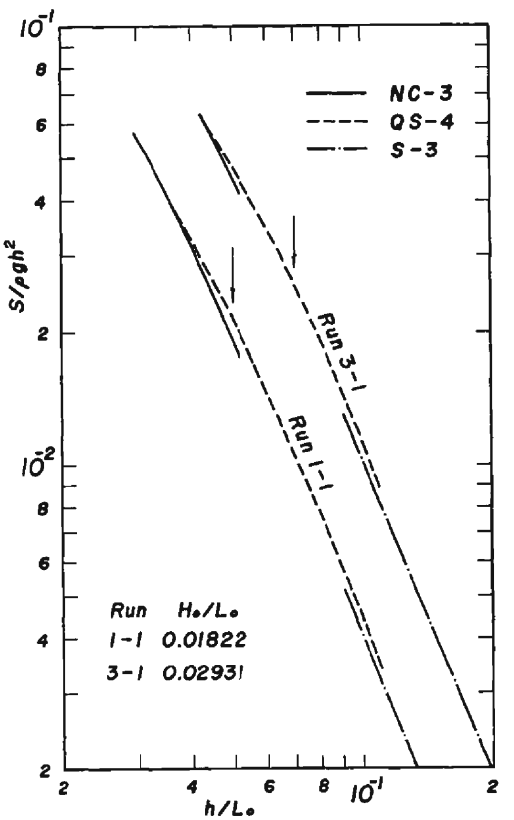

Fig. 13 Changes in radiation stress.

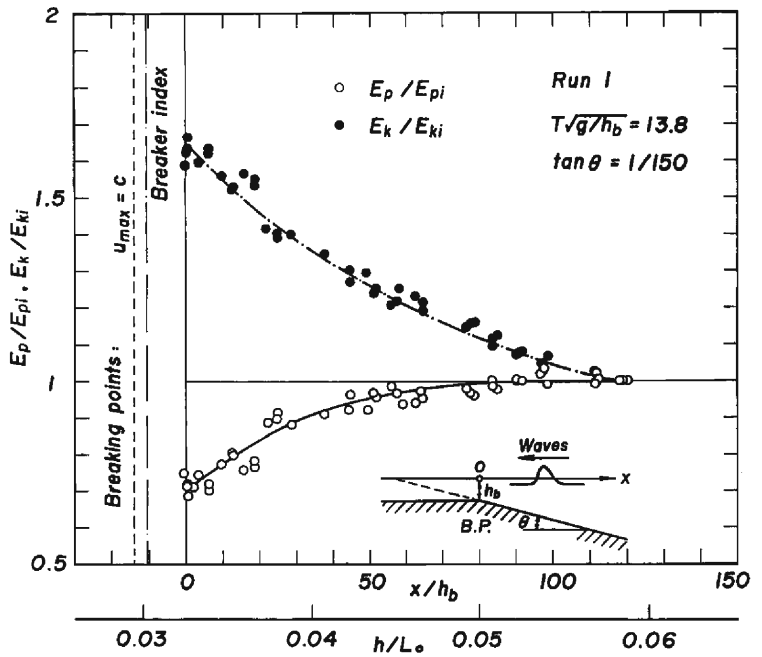

(1) Run 1

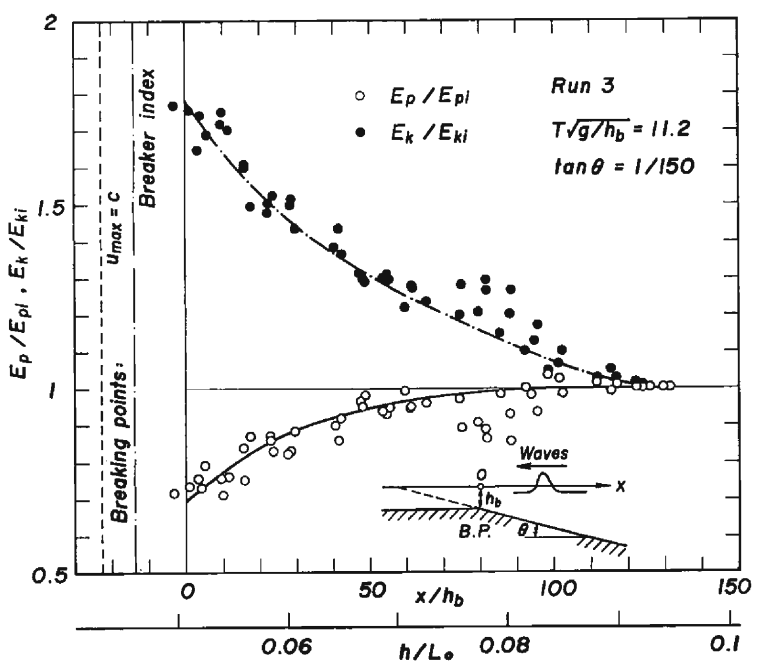

(2) Run 3

Fig. 14 Changes in potential and kinetic energies over the slope.

takes a maximum value.

The experimental results of the changes in wave energies, E_p/E_{pi} and E_k/E_{ki}, are shown in **Fig. 14**, in which the open and solid circles indicate the potential and kinetic energies respectively. The experimental values of the kinetic energy in this figure are calculated from Eq. (24) using the experimental values of the wave length and potential energy.

Certain fluctuations arise in Run 3 within $80<x/h_b<95$ because of weak meandering of waves. However, it is remarkable that the potential energies gradually increase in the offshore region, $x/h_b<100$ like does the theoretical estimation and turn into the slight decrease until 50 to 60 of x/h_b. They begin to decrease sharply at these points. We now define the points where the potential energy turns from increase to decrease and begin to decrease sharply as the turning and initiating points, respectively. For Run 1 the breaking depth, h_b, and wave length, L_b, approximately equal 5.12 cm and 78 cm, respectively, so that the turning and initiating points of the potential energy, x_t/L_b and x_i/L_b, nearly equal 6.6 and 3.6, respectively. In Run 3 the potential energy begins to decrease sharply before the breaking point as Run 1. These two points, x_t/L_b and x_i/L_b, are about 8.6 and 3.6, respectively.

To justify the changes in wave properties based on assumption, Eq. (23) we now make some discussion on the changes in group velocity with the aid of the so-called stream function theory[14]. According to the stream function theory in the reference frame moving with the wave velocity, the surface displacement of a wave is given as

$$\left.\begin{aligned}\eta=\frac{1}{c}\Bigg(\Psi_0-\sum_{n=4,6,\cdots}^{N-1}&\sinh(n-2)\pi\frac{h+\eta}{L}\\&\times\left\{X_n\cos(n-2)\pi\frac{x_1}{L}+X_{n+1}\sin(n-2)\pi\frac{x_1}{L}\right\}\Bigg)\end{aligned}\right\}\quad\cdots\cdots(26)$$

where $x_1=x-ct$, N_is an odd number, ψ_0 the stream function at the wave surface, and X_j are coefficients of the Fourier series. There exists a problem in adopting the theory to estimate wave properties over a slope. Because the stream function is a constant only in the reference frame of the wave, measured surface displacements in time are able to satisfy the role of those in space only when the wave propagates on water of uniform depth. On the other hand, for the wave on a slope surface displacements in space must be used in Eq. (26). Therefore, at this stage we deal with the stream function in a different manner from usual. The parameters in the stream function are determined so as to strictly satisfy the kinetic boundary condition with errors of the order of 10^{-4} to 10^{-5} using measured values of wave periods and wave lengths. The gross errors for the dynamical boundary condition are evaluated by the variance

$$\left.\begin{aligned}E_d&=\frac{1}{I}\sum_{i=1}^{I}(\overline{Q}-Q_i)^2\\\overline{Q}&=\frac{1}{I}\sum_{i=1}^{I}Q_i\end{aligned}\right\}\quad\cdots\cdots(27)$$

$$Q_i=\eta_{mi}+\frac{1}{2}\{(u_i-c)^2+w_i^2\}$$

where Q_i are the Bernoulli constants at the wave surface, and the subscript i is a phase index for a sequence consisting of I values. Resultant errors of the dynamical boundary condition are in the range of 10^{-3} to 10^{-4}.

Fig. 15 shows the changes in group velocity over the slope of 1/150, where the group velocity is defined as the ratio of the wave energy flux to total energy. The solid lines in the figure are experimental curves of wave velocities, c/c_i. As the kinetic energy is extremely sensitive to asymmetry of wave profiles, estimated values of group velocities, c_g/c_{gi}, have certain fluctuations in the offshore region with resemblance to wave profiles as shown in **Fig. 6**.

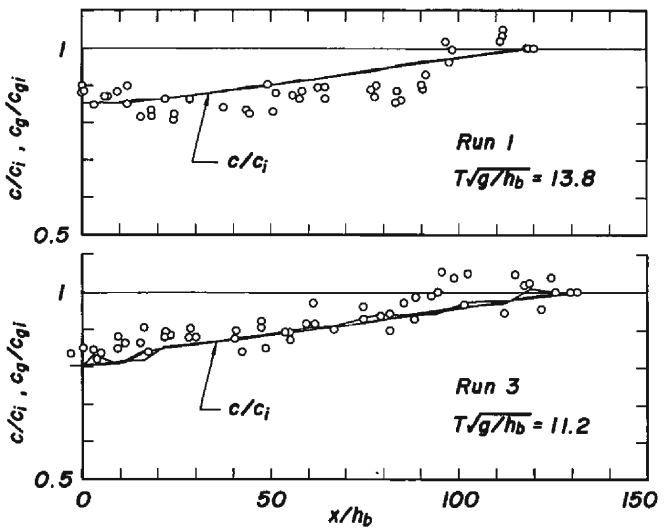

Fig. 15 Changes in group velocity over the slope based on the stream function theory.

The changes in kinetic energy, $(E_k/E_{ki})_s$, are shown in **Fig. 16**, which are evaluated by Eq. (5). In the figure the subscript s denotes the values based on the stream function theory, and the chain lines are experimental curves of E_k/E_{ki} based on Eq. (5). The values of $(E_k/E_{ki})_s$ take values of less than unity in the offshore region, but both $(E_k/E_{ki})_s$ and E_k/E_{ki} reasonably coincide together with experimental errors of wave velocities, c/c_i, in regard to group velocities, c_g/c_{gi}. **Figs. 15** and **16** demonstrate that the assumption, Eq. (23), is well satisfied by shallow water waves over the slope of 1/150. Furthermore, the changes in potential energy, $(E_p/E_{pi})_s$, are quite agree with those shown in **Fig. 14**, satisfying the kinetic boundary condition.

Comparing **Fig. 12** with **Fig. 14** gives a remarkable difference between the experimental and theoretical results, showing an abrupt decrease in potential energy before the waves break. Furthermore it is notable that the abruptly decreasing

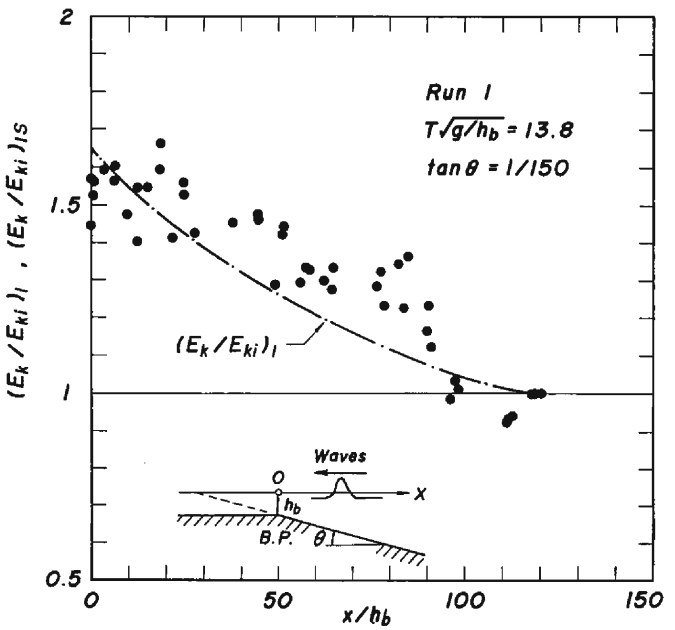

(1) Run 1

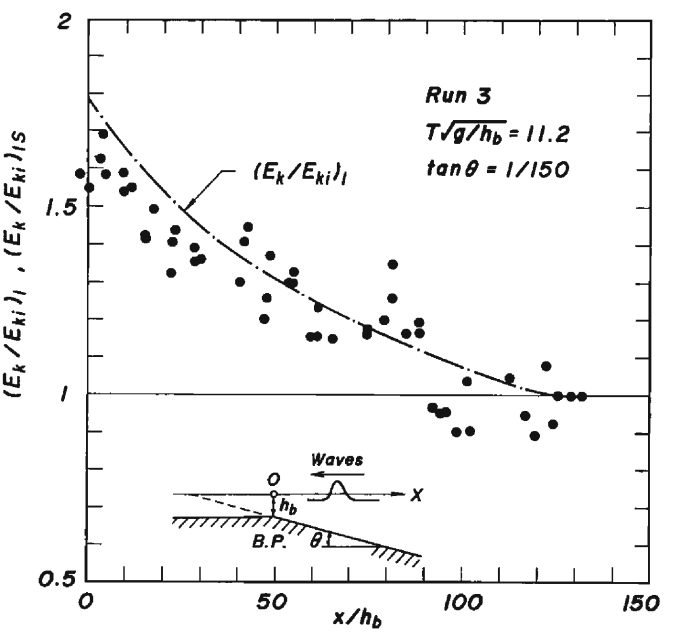

(2) Run 3

Fig. 16 Changes in kinetic energy over the slope based on the stream function theory.

point is nearly equal to the point where the radiation stress takes a maximum value. An experimental tendency that the kinetic energy increases as the wave approachs the breaking point, is the same as the theoretical tendency. However the experimental increasing rates of kinetic energy are several times the theoretical ones because of the abrupt decrease in potential energy.

Next, let us investigate the wave set-down which is caused by the changes in radiation stress. It is greatly concerned with the breaking of waves. **Fig. 17** shows experimental results of the wave set-down, in which the curves are the theoretical estimations of the wave set-down and radiation stress. Experimental and theoretical wave set-down are roughly agreeable in the deeper region. But the former is larger over the whole range of distance and about three times of the latter near the breaking point, that is, the values are rather the same as the radiation stress. The true wave set-down sensitively depends on how the mass flux of waves balances the discharge resupplied through the circulating duct in the wave tank. Therefore the chief reason may come from the fact that the mass flux is slightly larger than the resupplied discharge. This is resemblance to the tendency that experimental wave lengths are shorter and breaking points are consequently located more seaward than the theoretical ones.

Investigating the experimental results in detail, it is noted that the wave set-down

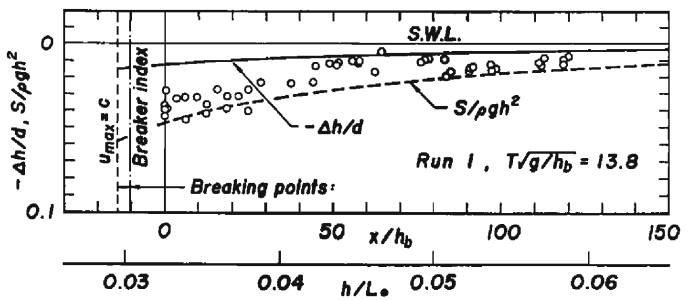

(1) Run 1

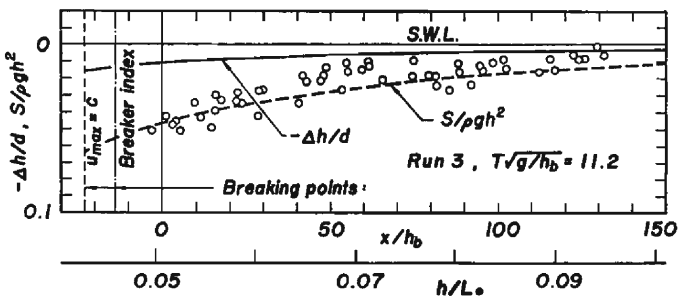

(2) Run 3

Fig. 17 Changes in wave set-down over the slope.

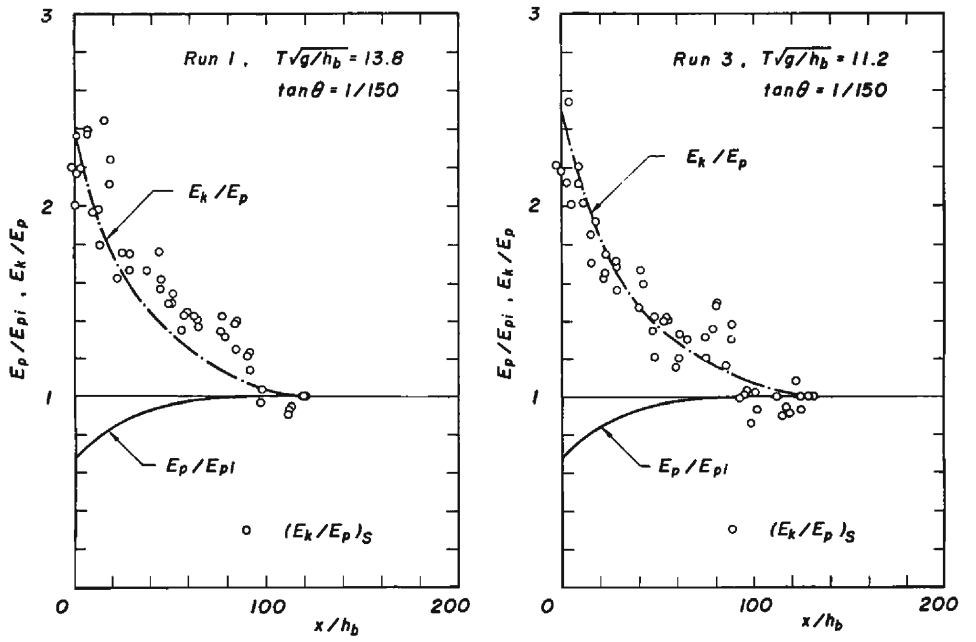

(1) Run 1 (2) Run 3

Fig. 18 Partition rates of wave energies.

begins to change sharply near the initiating points of 50 to 60 of x_i/L_b the same as the potential energy and radiation stress.

Fig. 18 shows the partition of wave energies, which is defined as the ratio between the kinetic and potential energies, E_k/E_p, and is obtained from the experimental curves shown in **Fig. 14**. Corresponding values of $(E_k/E_p)_s$, based on the stream function theory and Eq. (6), are also shown in the figure. Both values of E_k/E_p and $(E_k/E_p)_s$ give fairly good agreement as **Fig. 16**. The ratios, E_k/E_p, approximately equals 2.4 at the breaking points. These results conclusively show that kinetic energy is extremely predominant when the wave breaks.

From the above discussion, we conclude that the radiation stress, S/S_i, takes a maximum value and at the same time the potential energy also begins to decrease toward the breaking points, resulting in the break of the energy balance in waves, and that this phenomena has significant effects upon the breaking of waves. The imbalance in the partition rate of wave energies is confirmed as a premonitory phenomenon of the breaking of waves.

5. Conclusion

The breaking of waves may be subjected to not only the local hydrodynamical condition such as the so-called Rankine-Stokes' breaking condition and the occurrence

of cusp on the wave crest at just breaking but also the inner breaking conditions which integrate the properties of waves.

In the present paper, the changes in potential energy due to wave shoaling have been investigated experimentally, and the dynamical breaking condition has been discussed based on the imbalance in the partition of wave energies. The most significant result is concluded as follows;

When waves propagate and approach the breaking point, the potential energy in waves abruptly begins to decrease in front of the breaking point. On the contrary, the kinetic energy abruptly increases because of the decrease in potential energy, and becomes extremely predominant. As a result, the partition rate of wave energies becomes imbalanced and waves fall into the unstable state as a whole. Finally, this may lead to the breaking of waves.

Acknowledgements

This paper is part of the co-operative investigations during S. Tsutsui's stay at the Disaster Prevention Research Institute, Kyoto University, as an internal research worker of the Ministry of Education, Science and Culture, in 1979, and also is partly supported by the Grant-in-Aid for Scientific Research of the Ministry.

We thank Mr. H. Hiraguchi, Graduate student, and the staff of the Ujigawa Hydraulics Laboratory, Disaster Prevention Research Institute, for their great assistance in this experiment.

References

1) Stokes, G. G.: On the theory of oscillatory waves, Trans. Cambridge Phil. Soc., Vol. 8, 1847, pp. 197–229.
2) Longuet-Higgins, M. S.: The generation of capillary waves by steep gravity waves, Jour. Fluid Mech., Vol. 16, 1963, pp. 138–159.
3) Greenspan, H. G.: On the breaking of water waves of finite amplitude on a sloping beach, Jour. Fluid Mech., Vol. 4, 1958, pp. 330–334.
4) Goda, Y.: A synthesis of breaker index, Proc. JSCE, Vol. 180, 1970, pp. 39–49 (in Japanese).
5) Cokelet, E. D.: Steep Gravity waves in water of arbitrary uniform depth, Proc. Roy. Soc. London., A, Vol. 286, 1977, pp. 183–230.
6) Longuet-Higgins, M. S. and R. W. Stewart: Radiation stress and mass transport in gravity waves, with application to "surf-beat", Jour. Fluid Mech., Vol. 13, 1962, pp. 481–504.
7) Skjelbreia, L.: Gravity waves, Stokes' third order approximation, tables of functions, Council on Wave Research, The Engineering Foundation, ASCE, 1959, 337p.
8) Tsuchiya, Y. and T. Yasuda: Quasi-Stokes wave theory by the reductive perturbation method, Proc. 25th Nat. Conf. on Coastal Engrg. in Japan, JSCE, 1978, pp. 6–9 (in Japanese).
9) Tsuchiya, Y. and T. Yasuda: A study on the new cnoidal wave theory, Proc. 21th Nat. Conf. on Coastal Engrg. in Japan, JSCE, 1974, pp. 65–71 (in Japanese).
10) Yasuda, T.: Studies on finite amplitude wave theories in shallow water, with validity of applications, Doctoral dissertation, Kyoto Univ., 1978, 145p (in Japanese).
11) Whitham, G. B.: Mass, momentum, and energy flux in water waves, Jour. Fluid Mech., Vol. 12, 1962, pp. 135–147.
12) Tsuchiya, Y., S. Tsutsui, T. Yasuda, T. Yamashita and H. Hiraguchi: Mass transport of breaking

waves, Proc. 27th Nat. Conf. on Coastal Engrg. in Japan, JSCE, 1980, pp. 45–49 (in Japanese).
13) Schwartz, L. W.: Computer extension and analytic continuation of Stokes' expansion for gravity waves, Jour. Fluid Mech., Vol. 62, 1974, pp. 553–578.
14) Dean, R. G.: Stream function representation of nonlinear Ocean waves, Jour. Geophysical Research, 1965, pp. 4561–4572.